J. Ocean Eng. Mar. Energy
DOI 10.1007/s40722-017-0079-5

RESEARCH ARTICLE

Harnessing wave power in open seas II: very large arrays of wave-energy converters for 2D sea states

Dali Xu[1] · **Raphael Stuhlmeier**[2] · **Michael Stiassnie**[2]

Received: 31 October 2016 / Accepted: 6 March 2017

Abstract Recently, Stiassnie et al. (J Ocean Eng Mar Energy 2(1):47–57, 2016) studied the potential for capturing wave energy over a large ocean basin via a toy model of a wave farm attacked by unidirectional wave fields. In the present work, we develop an approach to model macroscopically the behaviour of sparse arrays consisting of infinite rows of floating, axisymmetric wave energy converters in deep water. This approximate framework allows for such arrays to be characterized by frequency- and direction-dependent transfer functions. The example of a self-reacting converter consisting of vertically floating, coaxial cylinders moving in three modes of motion is discussed in detail, and the performance of large arrays of such devices, attacked by directional JONSWAP spectra and taking into account wave growth by the wind is investigated. This allows for fast and flexible estimates of power absorption by arrays as well as of their effects on the wave field.

Keywords Wave power · WEC arrays · Deep water · Floating point absorbers · Directional sea states

This research was supported by the Israel Science Foundation (Grant 464/13).

✉ Michael Stiassnie
miky@technion.ac.il

Dali Xu
xudl@shmtu.edu.cn

Raphael Stuhlmeier
raphaels@technion.ac.il

[1] College of Ocean Science and Engineering, Shanghai Maritime University, Shanghai 201306, China

[2] Faculty of Civil and Environmental Engineering, Technion–Israel Institute of Technology, Technion City, 32000 Haifa, Israel

1 Introduction

The current state of wave-power conversion is focused heavily on the design and operation of individual converters, and major steps have been made in recent years in turning the theoretical promise of wave power dating back to the 1970s into working devices that are now being tested at sea. The future of wave-driven renewable energy will require an intensification of these efforts: some designs, such as overtopping devices or oscillating water columns (OWCs) (see Falcão 2010), may be scaled up to increase production. For such devices, which need not move with the waves, increasing their size may be a viable way to increase captured power and decrease stresses on the device. To give but two examples, one of the earliest grid-connected wave-power devices, the LIMPET OWC, has been installed on land, and the Wave Dragon overtopping device is designed with a displacement of some 30,000 tons and tip-to-tip length of 300 m, so as to reduce the device response to waves (see Cruz 2008).

For floating-body devices, which capture power from motion driven by the incoming waves, their size (or the size of their individual moving elements) is limited by the lengths of the waves normally encountered. Such designs fall largely into three classes, consisting of either attenuators (long axis in the direction of wave propagation), terminators (long axis perpendicular to the direction of wave propagation), or point absorbers (small devices able to absorb power independent of the incident wave direction). Studies on attenuators and terminators by Bódai and Srinil (2015) and Kraemer and McCormick (2004) have quantified the intuitive observation that the optimal device dimension for heave or pitch motions must be considerably smaller (e.g., by a factor of about five for pitch response) than the incident wavelength. The same is true in broad terms for point absorbers, which rely on motion to generate large forces and moments for energy extraction.

Published online: 22 March 2017

In such cases, an overall increase in captured power can come about only through deploying many devices. One may expect in the long-term that such large, floating wave-power farms will be deployed far offshore, to exploit the more powerful wave regimes of deep water environments (see Stiassnie et al. 2016).

Driven by the vision of future large-scale energy harvesting from waves in the open seas, it is our intention to develop an approximate theory to aid in assessment of the resource and estimate impacts on the wave climate. Theoretical studies of arrays of floating bodies with a view towards power absorption go back to work in the 1980s by Falnes (1980), Thomas and Evans (1981), and others, and many exact theoretical results on array performance have been established (a review of recent progress is given by De Chowdhury et al. 2015). Arrays of bottom mounted oscillating wave surge converters have also received considerable attention in recent years (Sarkar et al. 2014; Michele et al. 2015; Noad and Porter 2015).

However, much current work on arrays of wave-energy converters (WECs) is restricted by virtue of the large computational costs to rather few devices, e.g., (Child and Venugopal 2010) consider 5 WECs, (Borgarino et al. 2012) between 9 and 25 WECs, (Sinha et al. 2016) 12 WECs, and (Folley and Whittaker 2009) 2 WECs, respectively, in their arrays. Various methods may be employed to reduce these computational costs, with a recent approach by Göteman et al. (2015b) enabling an analysis of arrays of more than 1000 heaving point absorbers by neglecting the interaction due to scattered waves, and in a later study (Göteman et al. 2015a) by introducing a cut-off distance for the interaction.

While there is much to be gained from further studies on optimizing array configurations, the practical considerations specific to deep water dictate a different approach. Deep-ocean devices will not only need to be considerably larger (both from an energy extraction as well as a survivability standpoint, see Xu et al. 2016) but will require a significant separation distance due to their large watch circle. This watch circle (also called drift circle) introduces a degree of uncertainty into the WEC location, which makes an array configuration based on optimizing interaction inappropriate. A large body of work also points towards the sensitivity of optimal array configurations to changes in frequency and direction of waves (Borgarino et al. 2012), to imperfect power take-off (PTO) control (Folley and Whittaker 2009), and other factors (see the discussion in McGuinness and Thomas 2015), which are compounded for widely spaced arrays in deep water.

The approach put forward here requires knowledge only of the hydrodynamics of a single, axisymmetric device, with the intention of providing a particularly accessible approximation for arbitrary line arrays (with a long axis perpendicular to the principal direction of wave incidence). A similar approach was followed for very compact arrays (with WECs attached to a rigid structure) by Garnaud and Mei (2010), who gave homogeneous transmission and reflection coefficients as functions of wavenumber for their array configuration. That a need exists for such simple, ready-to-use array models is clear from some recent investigations of WEC effects on wave climate, where various other simplifications have perforce been adopted, such as approximating wave-power arrays by porous structures with different porosity levels (Venugopal and Smith 2007), or by ad hoc modeling of devices as linear spring dampers (Smith et al. 2012). The approach proposed herein allows for an initial assessment of the extractable wave-power resource, and the effect of WEC arrays on the wave climate, in a simple, easily scalable way. In contrast to other approximate methods (e.g., Göteman et al. 2015b), our methodology allows for directional spectra, and requires no recalculation when the incident wave field is altered.

Our use of axisymmetric WECs allows each individual device to capture energy independent of the incident wave direction. Considering first a line of devices allows for a meaningful definition of "reflection" and "transmission", and multiple lines subsequently make up an array. For the large device spacings considered, and allowing for a range of wavenumbers and incident wave directions, it is appropriate to neglect array interactions (Borgarino et al. 2012). Indeed, Zeng and Tang (2013) report in a detailed study of arrays of truncated cylinder WECs that hydrodynamic coefficients for WECs spaced 50 radii apart are essentially indistinguishable from those for an isolated converter.

This paper is structured as follows: in Sect. 2, we present the basic equations of linear wave theory as they apply to our modeling of individual devices, and describe the geometrical setup of our arrays. In Sect. 3, we first cover fundamentals of wave structure interaction, and subsequently, present the general formulation to define reflection from a structure, the key point of our approach, and transmission through a line of structures. Section 4 covers the behaviour of a sparse array of floating twin-cylinder WECs, discussing hydrodynamics and relevant design considerations, as well as power reflection and transmission for this example. Section 5 takes up the example of Stiassnie et al. (2016) and examines the potential for harvesting wave power via arrays of twin-cylinder WECs in a long ocean basin under the influence of the wind. Section 6 provides a discussion of the results along with further examples. Some concluding remarks are given in Sect. 7, and the Appendix gives some tabulated values of reflection and absorption for the WEC arrays developed from the example of Sect. 4.

2 Physical and geometrical preliminaries

As is customary in the theory of wave–structure interaction in general (see, e.g., Newman 1977), and in large part in the analysis of wave-energy devices, our analysis is based on the linearised equations for an incompressible fluid and an inviscid flow. For an irrotational fluid motion, the velocity field is given in terms of a potential $\Phi(x, y, z, t)$, with t denoting time, whereupon conservation of mass requires

$$\nabla^2 \Phi = 0. \tag{1}$$

We must add boundary conditions on all interfaces of the fluid. These are

$$\Phi_{tt} + g\Phi_z = 0 \text{ on the mean free surface, and} \tag{2}$$

$$\Phi_z = 0 \text{ on the sea bed } z = -h, \tag{3}$$

where g is the acceleration of gravity. In addition, interfaces between the fluid and a structure must satisfy

$$\frac{\partial \Phi}{\partial n} = V_n \text{ at the equilibrium position of the structure's surface,} \tag{4}$$

i.e., the normal velocity of the structure must equal that of the adjacent fluid particles (here, V_n is the component of the structure's velocity in the direction of the outward pointing normal vector n).

We have called the arrays under consideration "line arrays" to invoke the fact that they consist of multiple lines of axisymmetric absorbers, which will subsequently necessitate the use of both Cartesian as well as cylindrical coordinates. Figure 1 presents a "top–down" view of the three scales involved in the problem. At the macroscale (left), the array consists of many lines with given reflection, transmission, and absorption properties. These are approximations of the more complex behaviour of an actual array (center), which consists of individual point absorbers (right). Assume that the point absorbers in each line are of the same type, and have a characteristic size q (here depicted by the radius). The (x, y)-plane represents the mean water surface, and the z-axis is assumed to point vertically upwards. The array is assumed to be of great extent in the y-direction, and waves are assumed to propagate principally in the x-direction. The incident waves may also attack the array obliquely, so that the wave fronts form an angle $\alpha \in [0, \pi/2)$ with the y-axis, and such that $\alpha = 0$ corresponds to normal incidence, with the caveat that our results become less accurate for very large angles (for $\alpha = \pi/2$, the array is essentially infinitely deep).

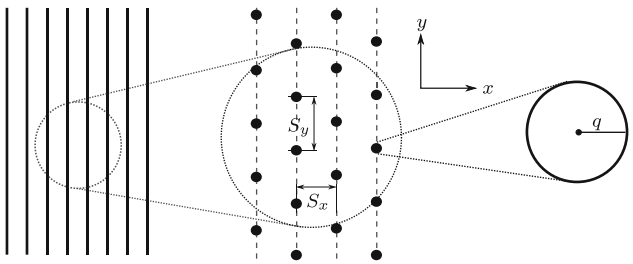

Fig. 1 Schematic depiction of the array: line array in the macroscale (*left*), individual absorbers in each line (*center*), and a single absorber of typical size parameter q (*right*). S_x and S_y are the device spacings in x and y directions, respectively

With reference to our stated goal of treating sparse arrays in deep water, the array spacing in the x-direction S_x, and that in the y-direction S_y are both taken much larger than the incident wavelength: $S_x,\ S_y \gg \lambda$. In Sect. 4, we shall see, through a concrete example, that design considerations for a floating point absorber perforce also require $\lambda \gg q$.

3 Behaviour of a sparse array of point absorbers

The attack of an incident wave on a structure has the effect of scattering waves from the structure, and setting the structure itself in motion, thereby causing it to radiate waves. For axisymmetric structures, only three modes of motion are possible: heave, sway, and roll. Furthermore, due to the assumption of linearity, the scattered waves may be calculated from the immobile structure at its equilibrium position and the total velocity potential for the problem is written as (see Newman 1977)

$$\Phi = \Phi_{\text{in}} + \Phi_{\text{s}} + (\Phi_{\text{he}} + \Phi_{\text{sw}} + \Phi_{\text{ro}}) = \Phi_{\text{in}} + \Phi_{\text{s}} + \Phi_{\text{r}}. \tag{5}$$

Here, Φ_{in} refers to the potential associated with the incident wave, while the scattered potential Φ_{s} is calculated from the fixed structure, and the radiation potentials are specified for heave (Φ_{he}), sway (Φ_{sw}), and roll (Φ_{ro}). The three radiation potentials are written together as Φ_{r}.

The incident wave is taken as a monochromatic plane wave with amplitude a_0, written in terms of the following velocity potential:

$$\Phi_{\text{in}} = \frac{iga_0}{2\omega} e^{kz} e^{-i(kr\cos\theta - \omega t)} + \text{c.c.}, \tag{6}$$

where r and θ are polar coordinates, k and ω are the wavenumber and frequency, related by $\omega^2 = gk,$, and c.c. denotes the complex conjugate. Under conditions of normal incidence ($\theta = 0$), this wave moves to the right in the positive x-direction.

Referring to Fig. 2, we introduce a cylindrical control surface A at distance r from the converter which will allow us to make a general accounting of the energy flux. The total

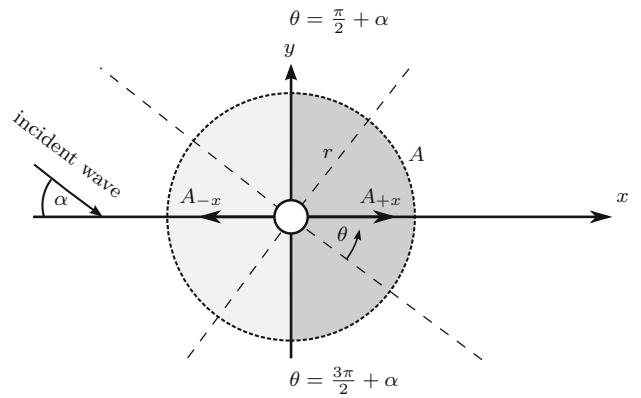

Fig. 2 Schematic depicting the control surfaces A (*dotted line*), A_{+x} (*right semicircle* of A), and A_{-x} (*left semicircle* of A) at a distance r from the converter, used for the balance of power for a wave incident at an angle α to the x-axis

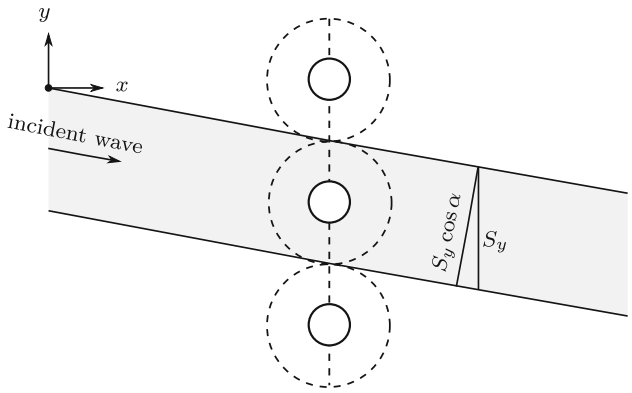

Fig. 3 Defining the "working area" (*shaded region*) for a single WEC in a line array with inter-WEC spacing S_y and angle of incidence α

energy flux through this surface is defined by Stoker (1992) as

$$\frac{\mathrm{d}E}{\mathrm{d}t} = \iint_A -\rho \frac{\partial \Phi}{\partial t}\frac{\partial \Phi}{\partial n}\mathrm{d}A, \tag{7}$$

where n denotes an outward pointing normal vector, and ρ is the density of water. The time-averaged energy flux (or power) through A is subsequently written as

$$P = \frac{\overline{\mathrm{d}E}}{\mathrm{d}t} = -\frac{\rho}{T}\int_{t_0}^{T+t_0}\int_{-\infty}^{0}\int_{\alpha}^{\alpha+2\pi}\frac{\partial \Phi}{\partial t}\frac{\partial \Phi}{\partial r}r\mathrm{d}\theta\mathrm{d}z\mathrm{d}t \tag{8}$$

which incorporates incident, radiated, and scattered terms of the potential (5). Here, $T = 2\pi/\omega$ is the wave period, t_0 is an arbitrary initial time, and the bar denotes a time average. Independent of the size of the control surface

$$P + P_\mathrm{a} = 0, \tag{9}$$

where P_a is the power absorbed by the device. Likewise, the control surface may be divided into halves A_{-x}, A_{+x} along the y-axis (see Fig. 2), with the corresponding power through each half denoted by P_{-x} and P_{+x}, respectively. Thus, (9) may be reformulated as

$$P_\mathrm{a} + P_{-x} + P_{+x} = 0. \tag{10}$$

The power through the left half-cylinder A_{-x} in Fig. 2 is defined by

$$\begin{aligned} P_{-x} &= -\frac{\rho}{T}\int_{t_0}^{t_0+T}\int_{\alpha+\pi/2}^{\alpha+3\pi/2}\int_{-\infty}^{0}\frac{\partial \Phi}{\partial t}\frac{\partial \Phi}{\partial r}r\mathrm{d}\theta\mathrm{d}z\mathrm{d}t \\ &\equiv -P_\mathrm{in} + P_\mathrm{re} \end{aligned} \tag{11}$$

where

$$P_\mathrm{in} = \frac{\rho}{T}\int_{t_0}^{t_0+T}\int_{\alpha+\pi/2}^{\alpha+3\pi/2}\int_{-\infty}^{0}\frac{\partial \Phi_{in}}{\partial t}\frac{\partial \Phi_{in}}{\partial r}r\mathrm{d}\theta\mathrm{d}z\mathrm{d}t. \tag{12}$$

The power through the right half-cylinder A_{+x} is defined by

$$P_{+x} = -\frac{\rho}{T}\int_{t_0}^{t_0+T}\int_{\alpha+3\pi/2}^{\alpha+\pi/2}\int_{-\infty}^{0}\frac{\partial \Phi}{\partial t}\frac{\partial \Phi}{\partial r}r\mathrm{d}\theta\mathrm{d}z\mathrm{d}t \equiv P_\mathrm{tr} \tag{13}$$

where θ is measured from the direction of incidence of the waves (see Fig. 2), and r is the radius of the control cylinder. Note that this defines P_re and P_tr, which are interpreted as the reflected and transmitted power, respectively. We note that P_re is independent of the radius of the control surface, provided this radius is large enough; however, this does not hold for P_in nor for P_tr.

Considering a line of converters with equal spacing S_y along the y-axis (see Fig. 3), we now fix the radius of the control surface $r = S_y/2$. It is then possible to write explicitly the incident power associated with a monochromatic wave incident at an angle α, using (6) and (12):

$$P_\mathrm{in} = \frac{1}{2}\rho g a_0^2 c_\mathrm{g} S_y \cos\alpha, \quad \text{with } c_\mathrm{g} = \frac{1}{2}\sqrt{\frac{g}{k}}, \tag{14}$$

where ρ is the density of water, c_g is the group velocity, k and ω are the wavenumber and angular frequency of the incident wave, and the water is assumed deep. The incident power passing through the segment of length S_y effectively decreases as the angle of incidence α increases.

From (10) to (13)

$$P_\mathrm{a} + P_\mathrm{re} + P_\mathrm{tr} = P_\mathrm{in}, \tag{15}$$

which allows for the definition of energetic absorption, reflection, and transmission coefficients

$$T_{\mathrm{a}} = P_{\mathrm{a}}/P_{\mathrm{in}} \tag{16}$$

$$T_{\mathrm{re}} = P_{\mathrm{re}}/P_{\mathrm{in}}, \tag{17}$$

$$T_{\mathrm{tr}} = P_{\mathrm{tr}}/P_{\mathrm{in}}, \tag{18}$$

which satisfy

$$T_{\mathrm{a}} + T_{\mathrm{re}} + T_{\mathrm{tr}} = 1. \tag{19}$$

These coefficients characterize the first line of absorbers, and depend on the angle α of wave incidence. The transmitted component is incident on the subsequent line, giving transmission and absorption coefficients for an array composed of N lines of point absorbers by

$$T_{\mathrm{tr},N} = (T_{\mathrm{tr}})^N, \tag{20}$$

$$T_{\mathrm{a},N} = \sum_{i=0}^{N-1} T_{\mathrm{a}} \cdot (T_{\mathrm{tr}})^i = T_a \frac{1-(T_{\mathrm{tr}})^N}{1-T_{\mathrm{tr}}}, \tag{21}$$

which provides a simple mechanism for approximating array performance, and is a main result. We note that this general result holds for any axisymmetric WEC, and does not depend on a particular device.

It is not possible to give any more general form for the absorbed power P_{a}. For floating-body devices, power is absorbed as a direct result of device motions, which must be calculated, and the power take-off has the effect of a damper. Unlike the general form for (11) or (13) above, writing the expression for the absorbed power requires a choice of WEC design (in particular, of WEC motions), and the computation of WEC hydrodynamics, either through analytical techniques, such as eigenfunction expansion, or alternatively via numerical tools, such as boundary element methods (e.g., WAMIT, NEMOH). In Sect. 4, such a concrete example of a self-reacting device composed of two floating cylinders is developed.

4 Arrays of floating-cylinder WECs

The framework for approximating a sparse line array was detailed in Sect. 3, and the main result (20)–(21) relies on the specification of curves for reflection (calculated from (11)) and absorption, as functions of frequency. Once the hydrodynamics of a single device are known, this information can be plugged into this framework and yield quick results with no additional computational effort. We will demonstrate this by means of concrete examples in the sections to come, using a system of two coaxial vertically floating cylinders moving in heave, sway, and roll, connected by a continuously distributed damper C which extracts energy from their relative motion (see Fig. 4).

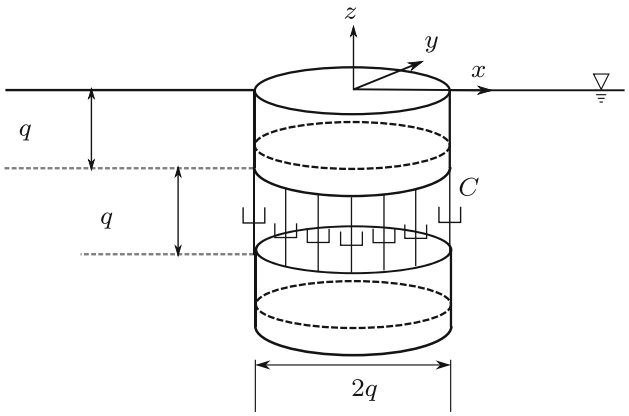

Fig. 4 Schematic depiction of the geometry of the floating twin-cylinder WEC, with radius, draft, and inter-cylinder spacing q, and a distributed damping coefficient C representing a PTO

4.1 WEC design and hydrodynamics

In keeping with our main message of studying wave-power harvesting in deep seas, the WEC considered is self-reacting (i.e., it relies on relative motion to generate power). The considerations involved in design and some necessary hydrodynamic properties are outlined briefly in what follows, and we refer the reader to Xu et al. (2016) for further details.

The design proceeds in two stages: determining the optimal size q for a given incident design wavenumber k_{d} based on the free (undamped) motions of the bodies, and subsequently determining the optimal damping coefficient C based on maximizing the power absorption given this converter size.

To reduce the number of parameters involved in the optimization, the radius and draft of each cylinder, and the inter-cylinder distance are taken equal to q. For flotational stability, the upper $2/3$ of each cylinder is assumed to have density $3\rho/4$, while the lower $1/3$ has density $3\rho/2$; hence, the cylinders are neutrally buoyant, and the moment of inertia of the cylinders may be calculated.

Considering the undamped motion, an incident monochromatic wave of given wavenumber k_{d} induces resonance in the roll mode (which is coupled to the sway mode) at a certain size q, and resonance in the heave mode for a larger converter size. For robustness of the converter, as well as to harness the larger and more efficient motions in the heave mode, this larger size $qk_{\mathrm{d}} = 0.65$ is chosen for all cylinders (see Xu et al. 2016). Evidence of the first absorptive peak (corresponding to a roll/sway optimum) may be found in Fig. 5 about $k/k_{\mathrm{d}} \approx 0.6$. Note that here and subsequently the power (absorbed, reflected, or transmitted) is presented in nondimensional form for ease of application. At the peak of absorption around $k = k_{\mathrm{d}}$, for example, the value given in Fig. 5 for a wave of $a_0 = 0.87$ m and $k_{\mathrm{d}} = 0.0653$ 1/m

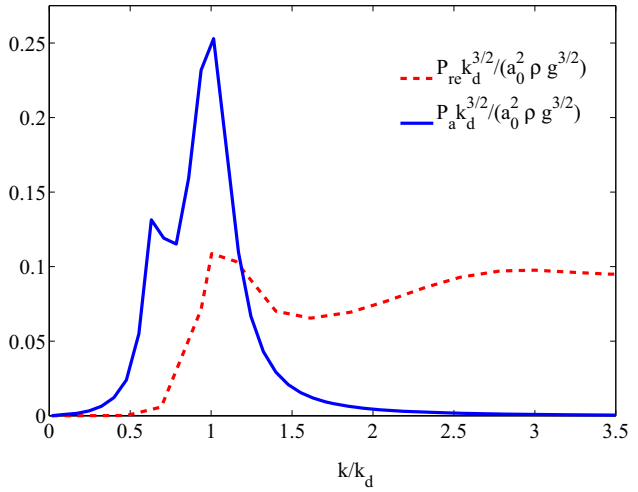

Fig. 5 Dimensionless absorbed power $P_{\mathrm{a}}k_{\mathrm{d}}^{3/2}/(a_0^2\rho g^{3/2})$ (*blue, solid line*) and dimensionless reflected power $P_{\mathrm{re}}k_{\mathrm{d}}^{3/2}/(a_0^2\rho g^{3/2})$ (*red, dashed line*) for a twin-cylinder WEC in heave, sway, and roll with size $qk_{\mathrm{d}} = 0.65$ and damping coefficients C chosen for optimal power absorption in heave (colour figure online)

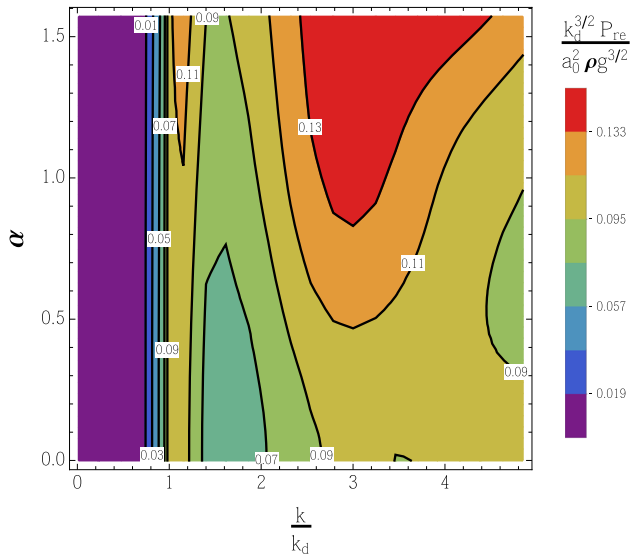

Fig. 6 Dimensionless reflected power $P_{\mathrm{re}}k_{\mathrm{d}}^{3/2}/(a_0^2\rho g^{3/2})$ of a twin-cylinder WEC attacked by a monochromatic wave with wavenumber k_{d} and amplitude a_0 incident at an angle α. $\alpha \in [0, \pi/2]$ is plotted on the vertical axis

would thus entail a power capture of some 350 KW for a device size $q = 10$ m.

For twin floating cylinders, the absorbed power comes from relative motion of the upper and lower cylinders

$$P_{\mathrm{a}} = \frac{1}{2}C\omega^2(\zeta_{z10} - \zeta_{z20})(\zeta_{z10}^* - \zeta_{z20}^*) + \frac{1}{4}C\omega^2 q^2(\theta_{10} - \theta_{20})(\theta_{10}^* - \theta_{20}^*), \tag{22}$$

where ζ_{zj0} is the complex amplitude of the vertical displacement, and θ_{j0} is the complex amplitude of the angle around the y axis. Throughout, * denotes a complex conjugate, and $j = 1, 2$ corresponds to the upper and lower cylinders. The cylinder size $qk_{\mathrm{d}} = 0.65$ then corresponds to a maximum of absorbed power when $Ck_{\mathrm{d}}^{5/2}/(\rho g^{1/2}) = 0.12$, as found by Xu et al. (2016). Comparing these results to computations for a single floating cylinder (which is assumed, artificially in deep water, to be attached to a fixed reference) shows that suspending a second cylinder two drafts below the water surface provides a very stable reference for cases when water depth precludes the use of the sea-floor. The dimensionless power absorption curves for a single and twin cylinders are strikingly similar, and exhibit an indistinguishable maximum at the tuning wavenumber.

4.2 Power reflection and transmission for floating-cylinder WECs

Having calculated the absorbed power (see (22) and Fig. 5), it remains to determine the reflected power from (11). The transmitted power and corresponding coefficients then follow from (19) for a specified spacing S_y, and for an array from (20) to (21).

The dimensionless reflected power for a single WEC as a function of incident wavenumber for normally incident ($\alpha = 0$) waves is shown in Fig. 5. This demonstrates a maximum of reflection at the tuning wavenumber $k = k_{\mathrm{d}}$ when device motions are largest, and demonstrates the relative transparency of the small device to longer waves $k/k_{\mathrm{d}} \ll 1$. The corresponding figure for obliquely incident waves is Fig. 6. Thus, the red, dashed curve in Fig. 5 is a cross section of Fig. 6 through $\alpha = 0$. Figure 6 depicts the contour lines of reflection from a twin-cylinder device when the angle of incidence α is allowed to vary between 0 and $\pi/2$. The numerical values in this figure are also given in tabulated form in the Appendix.

Axial symmetry of the device entails that the absorption characteristics are unchanged for different wave headings. However, the power reflected and transmitted with respect to each line does change with wave heading. In particular, for shorter waves (as demonstrated in Fig. 6), a steeper angle of attack results in greater reflection.

5 Wave-power harvesting in an ocean basin

In this section, we shall apply the framework for arrays of twin-cylinder floating wave-energy converters to the assessment of the extractable wave-energy resource in an ocean basin. A preliminary study using on a toy model of a WEC array, with power capture, transmission, and reflection based on a closed-form solution for twin floating plates was recently

given by Stiassnie et al. (2016). In what follows, the idealized unidirectional spectra of that work are replaced by directional spectra. The interested reader may refer to Stiassnie et al. (2016) or any number of textbooks, e.g., Holthuijsen (2008), for some background on fetch-limited wave growth.

For a basin of length $L = 2000$ km, and three prevailing, constant winds characterized by wind speeds $U_\mathrm{d} = 10$ m/s, $U_\mathrm{d}^- = 7.5$ m/s, and $U_\mathrm{d}^+ = 12.5$ m/s, we investigate the potential for capturing wave power via a series of arrays of twin-cylinder WECs. Incident upon the first array are JONSWAP spectra with a generalized Pierson's directional distribution (see Holthuijsen (2008), p. 164):

$$D(\theta) = \begin{cases} A_1 \cos^m(\theta) & \text{for } |\theta| \le 90^\circ \\ 0 & \text{for } |\theta| > 90^\circ \end{cases} \tag{23}$$

where $A_1 = \Gamma(1 + m/2)/(\sqrt{\pi}\Gamma(0.5 + m/2))$, Γ is the gamma function, and an intermediate directional spreading value of $m = 10$ is used throughout.

For a constant wind $U_\mathrm{d} = 10$ m/s, and a WEC with radius $q = 10$ m, the peak frequency of the fully developed sea (which occurs after a fetch of $f_\mathrm{d} = 350.7$ km) coincides with the absorptive peak of the WEC (see Fig. 5). $U_\mathrm{d} = 10$ m/s is thus termed the design condition. The inter-WEC distance is chosen as $S_y = S_x = 500$ m, which fixes the scale of sparse the array.

Due to the superlinear accumulation of incident energy flux with fetch, it is sensible to attempt to extract energy only after the wave field has become fully developed. Thereafter, the optimal selection of array depth $\delta = S_x \cdot (N - 1)$ (for N the number of lines in the array) and inter-array spacing Δd (see Fig. 7) becomes the primary issue. As is evident from (21), adding additional lines of converters to an array presents diminishing returns for the absorbed power (see Table 1). For the Pierson–Moskowitz (PM) spectra generated by U_d^-, U_d, and U_d^+, the theoretical maxima of absorption for an infinitely deep array are 0.65, 9.1, and 41.8 KW/m,

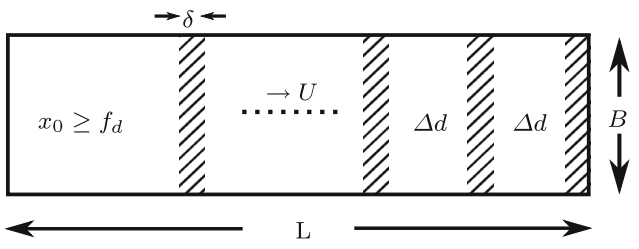

Fig. 7 Schematic geometry of an ocean basin of length L with a number of wave-farms (*shaded areas*) a distance Δd apart. A constant wind U blows from the *left*, and x_0 indicates the leading fetch prior to the first device, assumed greater than the fetch needed for a fully developed sea f_d under design conditions. $\delta = S_x \cdot (N-1)$ is the farm width, composed of N lines of absorbers, and B the harvesting breadth orthogonal to the wind direction

Table 1 Table showing diminishing returns in power absorption for an incident PM spectrum with $U_\mathrm{d} = 10$ m/s, for arrays composed of $N = 2, 3, 5$, and 10 lines

N	2	3	5	10
Rel. absorption	1.97	2.91	4.71	8.76

Relative absorption is given as a multiple of the absorption for a single line

respectively. These represent 14.8, 48.6, and 73.8% of the normal projection of all components of the incident energy flux, bearing in mind that the individual absorbers operate optimally for U_d. Table 1 illustrates this fact, showing that while two lines of converters may absorb nearly twice what a single line does, ten lines absorb less than nine times what a single line does. These losses accumulate due to both absorption and the assumed decay of reflected components, which propagate counter to the prevailing wind.

Over the inter-array space Δd, the constant wind causes the transmitted spectrum to grow, a process modelled via Miles' growth mechanism (see Stiassnie et al. 2016). Allowing sufficient fetch for the transmitted spectrum to regrow essentially to the incident spectrum (in fact, to 99% of the incident energy) under the design wind while limiting the growth of any frequency component from above by the corresponding PM spectrum, we find that the greatest overall power for a basin of length $L = 2000$ km may be generated by arrays $N = 10$ WECs deep.

For this configuration, evenly distributed arrays of WECs are installed over 1629.5 km, leaving a leading fetch of $x_0 = 370.5$ km over the 2000 km basin. For U_d, the incident wave-energy flux is 18.7 KW/m. The first line of the array absorbs some 214 W/m, with an entire array of ten lines absorbing 1.875 KW/m, or very nearly 10% of the available energy flux. Over subsequent $\Delta d = 58$ km of fetch, the wind U_d is allowed to regrow the waves, and a second array captures 1.84 KW/m. A slight diminution of incident energy between the arrays due to incomplete regrowth means that the 27th array, situated at the end of the basin, captures only 1.80 KW/m. A total of 48.92 KW/m may be captured in this manner under design conditions, installing 27 arrays each ten lines in breadth over 2000 km. The results when this array layout is held constant and the wind is allowed to vary are presented in Table 2, and may be compared to the results of the idealized, unidirectional case studied by Stiassnie et al. (2016).

While an array 10 lines deep may be optimal in terms of overall power capture, the fact that 27 arrays are needed over the course of the ocean basin may make it impractical on other grounds. As a second example, the number of lines in the array may be increased to 20, which allows for 14 arrays to be spaced evenly over the basin, with a leading fetch $x_0 = 375$ km. A summary of the results for the design wind U_d and

Table 2 Power absorption for arrays $N = 10$ and $N = 20$ lines deep, with spacing Δd dictated by the design wind $U_\mathrm{d} = 10$ m/s, calculated for varying winds

U_{10} (m/s)	7.5	10	12.5
Incoming energy flux (KW/m)	4.4	18.7	36.3
Power absorption for $N = 10$			
First array (KW/m)	0.14	1.88	3.81
Total (27 arrays) (KW/m)	2.7	48.9	135.3
Power absorption for $N = 20$			
First array (KW/m)	0.25	3.3	6.8
Total (14 arrays) (KW/m)	2.5	41.1	120.2

winds U_d^+, U_d^- is presented in Table 2. In each of the two example cases, the distribution of WEC arrays over an ocean basin has the potential to increase capture manyfold over a single array placed at the coast, supporting the conclusion reached in the companion paper (Stiassnie et al. 2016).

6 Discussion

The computational framework presented for quickly estimating the power absorbed by an array of axisymmetric converters, as well as the effects on the wave-field down wave of an array can be easily adapted to many other situations.

For example, employ the nondimensional device size $qk_\mathrm{d} = 0.65$ determined in Sect. 4.1 and a typical open ocean wave with $k_\mathrm{d} = 0.065\,\mathrm{m}^{-1}$ (equivalent to a wavelength $\lambda \approx 97$ m) with an amplitude $a_0 = 0.87$ m. This yields two cylinders with draft and radius 10 m, which (as in Sect. 5) is deployed in a line with $S_y = 500$ m to fulfil the assumption that the array is sparse.

For such a line of twin-cylinder devices attacked by normally incident waves, the absorption and transmission coefficients may be calculated from (16) to (18). For the benefit of the reader, a table of the relevant values in this case is given in the Appendix. Here, the entry for $\alpha = 0$, $k = k_\mathrm{d}$ can be used together with

$$T_\mathrm{a}(k; S_y) = \frac{4\tilde{P}_\mathrm{a}}{kS_y}, \quad T_\mathrm{re}(k; S_y) = \frac{4\tilde{P}_\mathrm{re}}{kS_y}. \tag{24}$$

to yields $T_\mathrm{a} = 0.03170$ and $T_\mathrm{tr} = 0.9549$, showing a single line array to be a relatively poor absorber, capturing just over 3% of the incident wave power of the monochromatic wave, while transmitting more than 95%.

Equation (20) makes it easy to extend these results to arrays composed of multiple lines. As an example, after 25 lines, the absorbed and reflected power can be seen to increase to 48.1 and 31.5 % of the incident power, respectively. This means that such a line array then absorbs $P_{\mathrm{a},N=25} = 11$ KW/m.

The scale-independent versatility of the methods may be demonstrated by a toy example describing numerically a wave-flume test of an array of small, floating-cylinder converters. Taking initially an incoming monochromatic wave of wavelength $\lambda = 0.5$ m, the results of Sect. 4 are applied. Our design considerations dictate a cylinder radius $q = 0.65k_\mathrm{d}^{-1} = 5.2$ cm. For such a small model of a floating-cylinder device, this means a volume of 434 cm^3, and because the cylinder is neutrally buoyant, a mass of 434 g and a damping of 0.560 Ns/m should be chosen to represent the selected PTO damping.

Assuming that the mechanically generated wave has an amplitude $a_0 = 1$ cm, in a flume with water of depth $h = 1$ m, its group velocity will be $c_\mathrm{g} = 44$ cm/s. Taking as a realistic example a flume of width 6 m, and constructing a test array consisting of three equally spaced converters per line, such that $S_y = 2$ m, from (14) the corresponding power (per meter wavefront of normally incident waves) will be 0.22 W/m.

For the first line of arrays, 94% of the incident wave energy is transmitted (see (18), and the Appendix), while 4.1% is absorbed by the damping elements. After three lines, we may apply (20) to see that transmission drops to 83% of the incident wave power, decreasing further to 78% with the addition of a fourth line. This simple example shows the versatility of our method in easily providing a numerical prediction for the behaviour of converter arrays in a wave flume, or on any other scale.

To return to the example of Sect. 5, for a constant design wind with speed $U_{10} = 10$ m/s and corresponding directional JONSWAP spectrum, the incoming energy flux per meter wave front is 18.7 KW/m. The maximum that an array of twin-cylinder converters tuned to the spectral peak may capture is 9.1 KW/m, or about 49%, requiring hundreds of lines of converters. A more reasonable bound, for a single array 50 lines deep, yields a capture of 5.8 KW/m, or 31%, and a reduction of the significant wave height by 40% behind each array. If an ocean basin of length 2000 km is utilized, six such arrays may be profitably deployed, increasing the capture to 33.9 KW/m, or some 5.8 times more than a single such array at the coast. However, a smarter deployment of converters, in 27 arrays each ten lines deep (which entails a 10% reduction in significant wave height behind each array) has been shown to lead to a capture of 48.9 KW/m, more than eight times the value for the single coastal array under the same conditions.

While the method presented is attractive for its computational simplicity, most other studies on the effects of large arrays of WECs rely either on ad hoc methods (as outlined in the "Introduction") or have different aims, making direct comparison of the results very difficult. One major challenge for the future consists in performing and making available experimental work on WECs and WEC arrays, so that numer-

ical results might be validated. Recently experimental results for large, dense arrays of buoys have been published by Stratigaki et al (2014), Weller et al (2010), and several others. Such results might profitably be compared with the approximations for very dense arrays discussed by Garnaud and Mei (2010), while comparison of the present results on sparse arrays must await further work.

7 Conclusions

Arrays of wave-energy converters garner more interest every day, as steps are taken to increase the readiness of WEC technology and move towards deploying grid-connected devices. Nevertheless, much groundwork is still being done, in assessment of the wave-energy resource, effects of energy converters on wave climates, and many other aspects of the technology. The intention of this work is to look further towards the future, at the deployment of WEC arrays in deep water, and to consider some of the consequences thereof.

As a result of moving to deep water, where one may attempt to exploit more powerful wave regimes, device sizes will correspondingly grow, as detailed in Xu et al. (2016). Device arrays will necessarily be sparse, as deep-water moorings dictate a large watch circle radius. Under these assumptions, we have undertaken to provide both a general framework for array calculations as well as several examples, including a detailed discussion for series of arrays in an ocean basin with realistic, wind-driven directional sea states which update the more simplified approach taken by Stiassnie et al. (2016). Unlike previous work, our model does not require any further computation for changing sea states, but allows for a "drop-in" application once the transmission and absorption of a line have been calculated from the potentials for a single device, making it ideal for inclusion in resource assessment studies.

For simple geometries, like the vertical cylinder, exact theories for infinite or semi-infinite lines of converters have been given by Linton and Evans (1990, 1992), Maniar and Newman (1997), and Chamberlain (2007) and others. All of these require significant numerical work to yield practical results. Other methods, which approximate some aspects of the array interactions, such as those developed by Göteman et al. (2015a, b) are eminently useful tools to study the smoothing effects of arrays and compare configurations from the point of view of power variability and cabling costs. Nevertheless, their implementation in wave-forecasting models to study the wave-power potential or model coastal impacts of large farms along the lines of Smith et al. (2012) is likely to be computationally very costly, as each change in wave conditions requires a recalculation of the array's behaviour. The examples presented herein demonstrate the versatility of our methods for treating arrays, and underline the need for further work on the potential for wave-power harvesting in the open oceans.

Appendix: Table of reflection and absorption coefficients

Table 3 supplements Fig. 6.

Table 3 Dimensionless reflected power $P_{\mathrm{re}}k_{\mathrm{d}}^{3/2}/(a_0^2\rho g^{3/2})$ and absorbed power $P_{\mathrm{a}}k_{\mathrm{d}}^{3/2}/(a_0^2\rho g^{3/2})$ of the twin-cylinder WEC attacked by obliquely incident monochromatic waves with wavenumber k and angle a (from 0° to 80°)

k/k_{d}	0.25	0.5	1.0	1.5	2.0	2.5	3.0	3.5	4.0
$\frac{P_{re}k_d^{3/2}}{a_0^2\rho g^{3/2}}$									
0°	2.09E−05	0.000155	0.109	0.0667	0.0744	0.0926	0.0981	0.0953	0.09774
10°	2.09E−05	0.000155	0.109	0.0673	0.0756	0.0947	0.101	0.0975	0.09807
20°	2.07E−05	0.000156	0.110	0.0690	0.0789	0.100	0.108	0.103	0.09930
30°	2.05E−05	0.000157	0.110	0.0715	0.0837	0.108	0.118	0.111	0.10172
40°	2.01E−05	0.000157	0.110	0.0748	0.0891	0.117	0.127	0.118	0.10511
50°	1.97E−05	0.000158	0.111	0.0784	0.0945	0.124	0.135	0.125	0.10907
60°	1.91E−05	0.000159	0.111	0.0821	0.0994	0.129	0.141	0.130	0.11398
70°	1.85E−05	0.000159	0.112	0.0859	0.103	0.133	0.146	0.137	0.12133
80 °	1.77E−05	0.000159	0.112	0.0897	0.107	0.136	0.150	0.145	0.13231
$\frac{P_a^* k_{\mathrm{d}}^{3/2}}{\rho g^{3/2}}$	0.00341	0.0308	0.258	0.0187	0.00438	0.00176	0.000855	0.000445	0.000241

References

Bódai T, Srinil N (2015) Performance analysis and optimization of a box-hull wave energy converter concept. Renew Energy 81:551–565

Borgarino B, Babarit A, Ferrant P (2012) Impact of wave interactions effects on energy absorption in large arrays of wave energy converters. Ocean Eng 41:79–88. doi:10.1016/j.oceaneng.2011.12.025

Chamberlain PG (2007) Water wave scattering by finite arrays of circular structures. IMA J Appl Math 72(1):52–66. doi:10.1093/imamat/hxl025

Child BFM, Venugopal V (2010) Optimal configurations of wave energy device arrays. Ocean Eng 37(16):1402–1417. doi:10.1016/j.oceaneng.2010.06.010

De Chowdhury S, Nader JR, Sanchez AM, Fleming A, Winship B, Illesinghe S, Toffoli A, Babanin A, Penesis I, Manasseh R (2015) A review of hydrodynamic investigations into arrays of ocean wave energy converters. arXiv:1508.00866

Cruz J (ed) (2008) Ocean wave energy. Springer, Berlin

Falcão AFdO (2010) Wave energy utilization: a review of the technologies. Renew Sustain Energy Rev 14:899–918

Falnes J (1980) Radiation impedance matrix and optimum power absorption for interacting oscillators in surface waves. Appl Ocean Res 2(2):75–80

Folley M, Whittaker T (2009) The effect of sub-optimal control and the spectral wave climate on the performance of wave energy converter arrays. Appl Ocean Res 31(4):260–266. doi:10.1016/j.apor.2009.10.006

Garnaud X, Mei CC (2010) Comparison of wave power extraction by a compact array of small buoys and by a large buoy. IET Renew Power Gener 4(6):519–530

Göteman M, Engström J, Eriksson M, Isberg J (2015a) Fast modeling of large wave energy farms using interaction distance cut-off. Energies 8(12):13,741–13,757. doi:10.3390/en81212394

Göteman M, Engstrom J, Eriksson M, Isberg J (2015b) Optimizing wave energy parks with over 1000 interacting point-absorbers using an approximate analytical method. Int J Mar Energy 10:113–126. doi:10.1016/j.ijome.2015.02.001

Holthuijsen L (2008) Waves in oceanic and coastal waters. Cambridge University Press, Cambridge

Kraemer D, McCormick M (2004) The effect of wavelength on the response of floating bodies. In: Sixth international conference on civil engineering in the oceans. American Society of Civil Engineers, Baltimore, p 255266

Linton CM, Evans DV (1990) The interaction of waves with arrays of vertical circular cylinders. J Fluid Mech 215(-1):549. doi:10.1017/S0022112090002750

Linton CM, Evans DV (1992) The radiation and scattering of surface waves by a vertical circular cylinder in a channelo. Philos Trans R Soc A Math Phys Eng Sci 338:325–357. doi:10.1098/rsta.1992.0011

Maniar HD, Newman JN (1997) Wave diffraction by a long array of cylinders. J Fluid Mech 339:309–330. doi:10.1017/S0022112097005296

McGuinness J, Thomas G (2015) optimal arrangements of elementary arrays of wave power devices. In: Proceedings of the 11th European wave and tidal energy conference

Michele S, Sammarco P, D'Errico M, Renzi E, Abdolali A, Bellotti G, Dias F (2015) Flap gate farm: from Venice lagoon defense to resonating wave energy production. Part 2: synchronous response to incident waves in open sea. Appl Ocean Res 52:43–61. doi:10.1016/j.apor.2015.05.002

Newman JN (1977) Marine hydrodynamics. MIT Press, Cambridge

Noad IF, Porter R (2015) Optimisation of arrays of flap-type oscillating wave surge converters. Appl Ocean Res 50:237–253. doi:10.1016/j.apor.2015.01.020

Sarkar D, Dias F, Renzi E (2014) Wave farm modelling of oscillating wave surge converters. Proc R Soc A Math Phys Eng Sci 470:20140,118–20140,118. doi:10.1098/rspa.2014.0118

Sinha A, Karmakar D, Guedes Soares C (2016) Performance of circular and concentric arrays of heaving point absorbers. Renew Energy 92:517–531. doi:10.1016/j.renene.2016.02.043

Smith HCM, Pearce C, Millar DL (2012) Further analysis of change in nearshore wave climate due to an offshore wave farm: an enhanced case study for the Wave Hub site. Renew Energy 40(1):51–64. doi:10.1016/j.renene.2011.09.003

Stiassnie M, Kadri U, Stuhlmeier R (2016) Harnessing wave power in open seas. J Ocean Eng Mar Energy 2(1):47–57. doi:10.1007/s40722-015-0038-y

Stoker JJ (1992) Water waves. Wiley, Hoboken. doi:10.1002/9781118033159

Stratigaki V, Troch P, Stallard T, Forehand D, Kofoed JP, Folley M, Benoit M, Babarit A, Kirkegaard J (2014) Wave basin experiments with large wave energy converter arrays to study interactions between the converters and effects on other users in the sea and the coastal area. Energies 7(2):701734

Thomas G, Evans D (1981) Arrays of three-dimensional wave-energy absorbers. J Fluid Mech 108:67–88

Venugopal V, Smith GH (2007) Wave climate investigation for an array of wave power devices. In: Proceedings of the 7th European wave and tidal energy conference, Porto, p 10

Weller SD, Stallard TJ, Stansby PK (2010) Experimental measurements of irregular wave interaction factors in closely spaced arrays. IET Renew Power Gener 4(6):628637

Xu D, Stuhlmeier R, Stiassnie M (2016) Parameter based design of a twin-cylinder wave energy converter for real sea-states. arXiv:1605.00428

Zeng XH, Tang SY (2013) The hydrodynamic interactions of an array of truncated circular cylinders as each cylinder oscillates independently with different prescribed modes. J Hydrodyn 25(1):27–38. doi:10.1016/S1001-6058(13)60335-2